Corrosion Science 222 (2023) 111410

Contents lists available at ScienceDirect

Corrosion Science

journal homepage: www.elsevier.com/locate/corsci

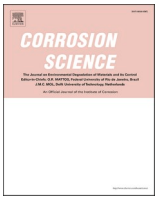

Sulphur diffusion through a growing chromia scale and effects of water vapour

Chuhan Sha [a], Limei Yang [b,c], Julie M. Cairney [b,d], Jianqiang Zhang [a,*], David J. Young [a]

[a] School of Materials Science and Engineering, University of New South Wales, Sydney, NSW 2052, Australia
[b] Australian Centre for Microscopy and Microanalysis, The University of Sydney, Sydney, NSW 2006, Australia
[c] School of Civil and Environmental Engineering, University of Technology Sydney, Sydney, NSW 2007, Australia
[d] School of Aerospace, Mechanical and Mechatronic Engineering, The University of Sydney, Australia

ARTICLE INFO

Keywords:
Chromia
Sulphur
Water vapour
Grain boundaries
High temperature corrosion

ABSTRACT

Fe-30Cr (wt%) alloy was exposed to Ar-0.5%SO_2 and Ar-10%H_2O-0.5%SO_2 gases at 650 °C, forming Cr_2O_3 scales. In dry SO_2 for 20 h, sulphur enrichment and scattered Cr-sulphides were observed at the scale-alloy interface, together with internal Cr-sulphide precipitates. After 100 h, sulphur disappeared from the interface, while more internal Cr-sulphides were produced. In wet SO_2, the sulphur enrichment and Cr-sulphides were maintained in both times, but no internal sulphidation was seen. Atom probe analysis revealed sulphur enrichment on chromia grain boundaries in both gases, to a greater extent in wet SO_2. These effects are discussed in terms of chromia grain boundary diffusion.

1. Introduction

Ferritic and ferritic/martensitic Fe-Cr alloys are of technical importance as critical components in high-temperature applications such as combustion power plants [1], gas cooled nuclear reactors [2], and other applications in the energy sector. Combustion processes and gasification of waste, biomass, coal, tars, etc. produce harsh service environments containing species such as CO_2, NO_x, H_2O, sulphurous gases, ash, and alkali chlorides, exposure to which lead to degradation of those Fe-Cr alloys [3,4].

Alloys based on Fe-Cr withstand high temperatures and corrosive environments by oxidising protectively, forming a dense and slowly growing Cr_2O_3 scale. Alloy design for this purpose based on Wagner's diffusion theory (i.e. the diffusion of reagents in the scale occurs via ion diffusion at a rate controlled by the diffusive properties of the oxide) [5] succeeds for oxygen and air exposure [6]. However, these alloys suffer breakaway oxidation when secondary oxidants such as C, S, Cl, H_2O, etc. are present [7–10]. Attention is focused here on the effects of sulphur.

For example, the simultaneous presence of sulphur and oxygen can produce metal sulphides and oxides, significantly compromising the effectiveness of protection afforded to Fe-Cr alloys at high temperatures, since the sulphidation rate is higher [11]. On the other hand, small amounts of SO_2 added to CO_2-H_2O gas can effectively reduce carbon penetration, and hence carbide formation beneath the oxide scale, a phenomenon suggested to result from preferential adsorption of sulphur on Cr_2O_3 grain boundaries [12]. Competitive oxidation/sulphidation reactions at high temperatures have been extensively investigated for low chromium alloys where breakaway oxidation prevails [13]. However, the role of SO_2 with and without H_2O is poorly defined for high chromium alloys. For this reason, the influence of these secondary oxidants on the growing Cr_2O_3 scale is the subject of this study.

Clearly, the pathways by which sulphur penetrates Cr_2O_3 scales are of interest, since the scales are dense and the solubility of sulphur in the solid oxide is negligible [14]. Identification of these diffusion paths is required in order to devise methods for preventing sulphur diffusion. The foreign species within a scale are dilute and nanoscale investigation is required to identify their locations. Recent studies using atom probe tomography (APT) revealed that carbon penetrates a pre-formed Cr_2O_3 scale along its grain boundaries, leading to internal carburisation beneath the scale [15,16]. The aim of the present study was to investigate segregation of sulphur inside Cr_2O_3 scales as well as across phase boundaries (gas-scale, scale-alloy) formed in dry and wet SO_2, by using transmission electron microscopy and atom probe tomography.

* Corresponding author.
E-mail address: j.q.zhang@unsw.edu.au (J. Zhang).

https://doi.org/10.1016/j.corsci.2023.111410
Received 5 May 2023; Received in revised form 29 June 2023; Accepted 16 July 2023
Available online 17 July 2023

2. Materials and experiments

A model alloy Fe-30Cr (wt%) was prepared by arc melting pure metals of Fe (99.98%, Sigma Aldrich) and Cr (99.995%, Sigma Aldrich) under a reducing Ar-5%H_2 gas atmosphere, using a non-consumable electrode. The cast alloy button was then annealed at 1100 °C for 50 h under flowing Ar-5%H_2 gas for homogenization. The button was then cut and ground into rectangular coupons approximately (1–1.5) × (7−9) × (8−10) mm in size and their surfaces ground to a 1200-grit finish. A small suspension hole was drilled near an edge. Prior to exposure, the alloy coupon was ultrasonically cleaned in ethanol. The unreacted alloy composition was confirmed by SEM/EDX (limit of detection of 0.1 wt%) as Fe-(29.7 ± 0.2)Cr (wt%).

The alloy coupon was mounted on a sample holder supported by a silica rod, and then transferred into the cold zone of an alumina tube reactor inside a horizontal tube furnace. Isothermal oxidation experiments were carried out at 650 °C in Ar-0.5%SO_2 and Ar-10%H_2O-0.5% SO_2 mixtures (vol%) with a linear flow rate of 2 cm/s and a total pressure of 1 atm, for a shorter time (20 h) and a longer time (100 h). The flow of Ar and SO_2 was regulated with Brooks mass flow controllers. Wet gases were generated by passing the Ar gas through a water bath to first produce an excess amount of water vapour that was then partially condensed at a controlled temperature set to yield the required water vapour concentration [17]. The wet Ar gas was mixed with SO_2 to obtain the desired gas composition before introducing it via trace-heated tubing into the reactor.

Equilibrium partial pressures of oxygen and sulphur calculated from FactSage 8.1 are shown in Table 1. After a stable reaction gas flow was established and the furnace was heated to 650 °C, the specimens were pushed into the hot zone. After reaction, the furnace was switched off and specimens were moved into the cold zone (200–300 °C) under flowing Ar gas until room temperature was reached.

A two-stage experiment was designed to examine whether SO_2 can penetrate a preformed Cr_2O_3 layer. The Fe-30Cr was reacted in Ar-10% H_2O for 20 h at 650 °C to form a Cr_2O_3 scale, and then the gas was switched to Ar-0.5%SO_2 for 20 h without changing the temperature.

Weight changes of reacted alloys were measured using an analytic balance (Mettler Toledo XP250) with an accuracy of 0.01 mg. Reacted specimens were characterised by scanning electron microscopy (SEM, Hitachi S3400), transmission electron microscopy (TEM, JEOL JEM-F200) equipped with an energy dispersive X-ray spectrometer (EDX, Pathfinder), and atom probe tomography (APT) with a picosecond-pulse ultraviolet laser (Cameca LEAP 4000X Si). TEM samples ~ 100 nm thick were prepared using a Xenon plasma focused ion beam microscope (ThermoFisher Helios G4 PFIB) with a maximum accelerating voltage of 30 kV for milling and 5 kV for cleaning. APT samples were also prepared by PFIB: bars of oxide layers parallel to the scale-alloy interface were lifted out and milled to produce ~60 nm diameter tips. The axis of the needle-shaped tips was parallel to the scale-alloy interface, to sample region of approximately uniform oxidant activities.

Data collection from the tip was carried out in the APT at a temperature of ~55 K, a laser pulse frequency of 250 kHz, a laser pulse energy of 70 pJ and a target detection rate of 0.5%. The APT data was reconstructed using Cameca software (AP Suite 6.1) by using the voltage change to estimate the radius evolution, the evaporation field of Cr, a k-factor of 3.3, and ICF of 1.56, and a detector efficiency of 52%. Rather large dataset of approximately 35 and 50 million ionic species were collected for reacted samples in dry and wet SO_2 gas after 100 h, respectively.

Table 1
Equilibrium minority gas partial pressures (atm) at 650 °C, 1 atm.

Species	Ar-10%H_2O	Ar-0.5%SO_2	Ar-10%H_2O-0.5%SO_2
SO_2	-	5.0×10^{-3}	5.0×10^{-3}
SO_3	-	3.5×10^{-9}	1.3×10^{-7}
O_2	5.0×10^{-9}	2.1×10^{-14}	3.0×10^{-11}
S_2	-	2.8×10^{-11}	1.4×10^{-17}
H_2	1.0×10^{-8}	-	1.3×10^{-7}
H_2S	-	-	1.7×10^{-13}

3. Results

3.1. Weight gains

Alloy weight gains after exposure at 650 °C in dry and wet SO_2 gases are given in Fig. 1. No scale spallation was observed during cooling or specimen handling. The alloy had higher weight gains in dry SO_2 than in wet SO_2 for both 20 h and 100 h reactions. For 20 h reaction, the weight uptake in dry SO_2 was ~0.10 mg/cm^2, whereas in wet SO_2 it was ~0.07 mg/cm^2. For 100 h reaction, the weight uptake in dry SO_2 increased only slightly to ~0.11 mg/cm^2, whereas in wet SO_2 it was ~0.08 mg/cm^2. It can be seen in Fig. 1 that the scaling rate in the initial stage (0–20 h) was higher than in the subsequent period (20–100 h).

3.2. Microstructure of corroded samples

3.2.1. Reaction after 20 h

Representative surface morphologies of Fe-30Cr exposed to dry and wet SO_2 for 20 h are shown in Fig. 2a and b. A scale surface consisting of oxide blades was observed for both conditions. The TEM cross-section (Fig. 3a) revealed the oxide scale grown in dry gas to consist of a dense oxide layer with oxide blades distributed on its surface. The average overall thickness (both dense layer and superficial layer of oxide blades) was ~ 450 nm, where an average thickness of ~180 nm was measured for the blade layer. Several pores were formed in the base alloy beneath the oxide scale, the large one shown with a lateral size of ~800 nm and a depth of ~300 nm.

Analysis of a selected area electron diffraction pattern (SAED) in the inset of Fig. 3a confirmed the scale to be Cr_2O_3 rhombohedral polycrystals. The size of individual grains is difficult to resolve from the bright-field TEM image, so dark-field imaging is used to highlight grains at selected orientations, allowing direct measurement of the grain size. Specifically, dark-field images were taken using a $\{10\bar{1}4\}$ reflection spot, to illuminate the corresponding grains, as shown in Fig. 3c. It was found the grains in Fig. 3b have a size of 15 ± 4 nm after exposure to dry gas for 20 h. Closely similar results were shown using other reflections (not shown).

The oxide scale grown in wet gas over 20 h (Fig. 3d) had a thinner dense oxide but thicker blade zone: ~340 nm for the overall oxide scale, and ~200 nm for the top blade. Smaller pores were found at the scale-

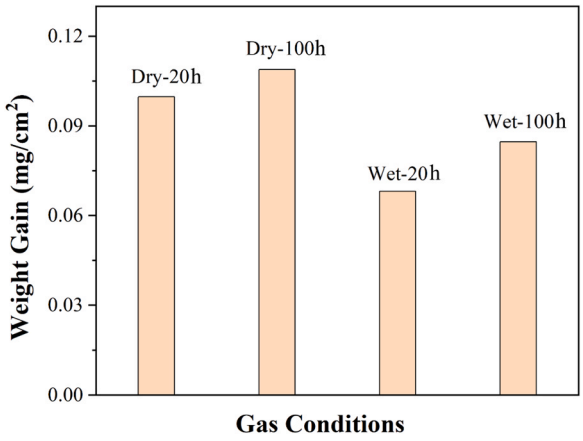

Fig. 1. Weight gains of Fe-30Cr after reaction at 650 °C in different conditions. Dry-20 h: Ar-0.5%SO_2-20 h; Dry-100 h: Ar-0.5%SO_2-100 h; Wet-20 h: Ar-10% H_2O-0.5%SO_2-20 h; Wet-100 h: Ar-10%H_2O-0.5%SO_2-100 h.

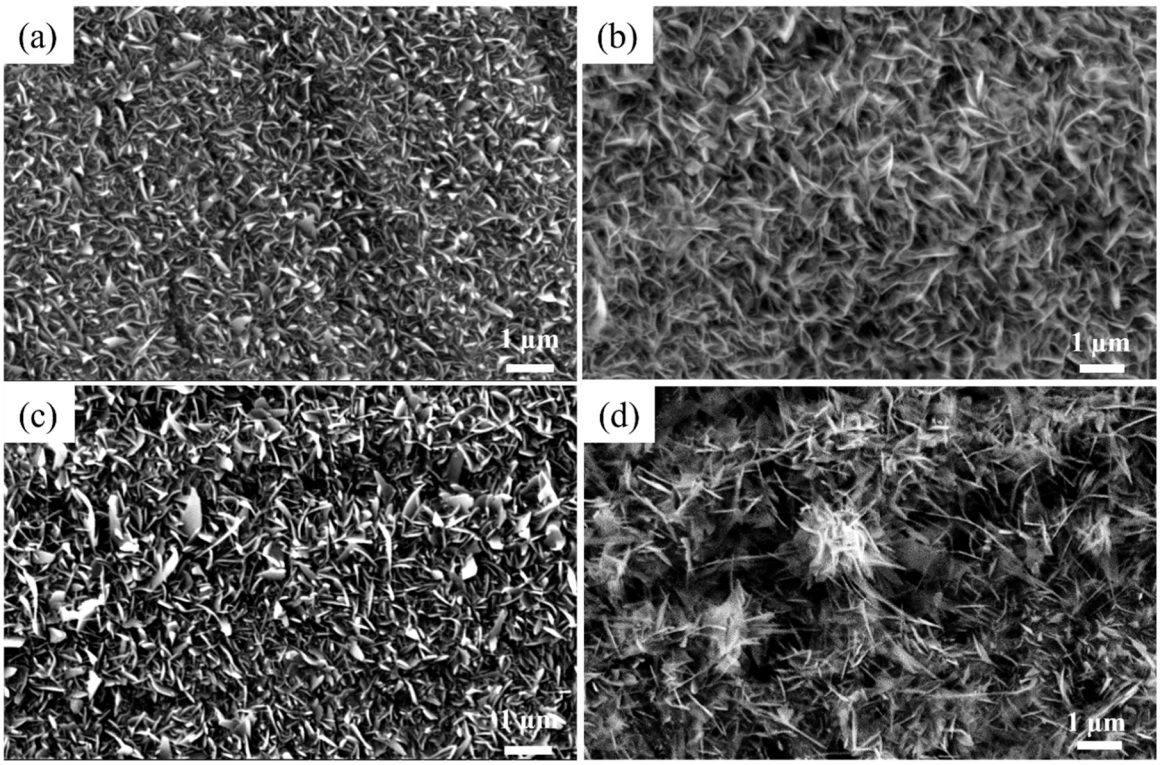

Fig. 2. SE (Secondary Electron)-SEM top view of Fe-30Cr reacted at 650 °C in (a) Ar-0.5%SO_2 for 20 h; (b): Ar-10%H_2O-0.5%SO_2 for 20 h; (c) Ar-0.5%SO_2-100 h (d): Ar-10%H_2O-0.5%SO_2 for 100 h.

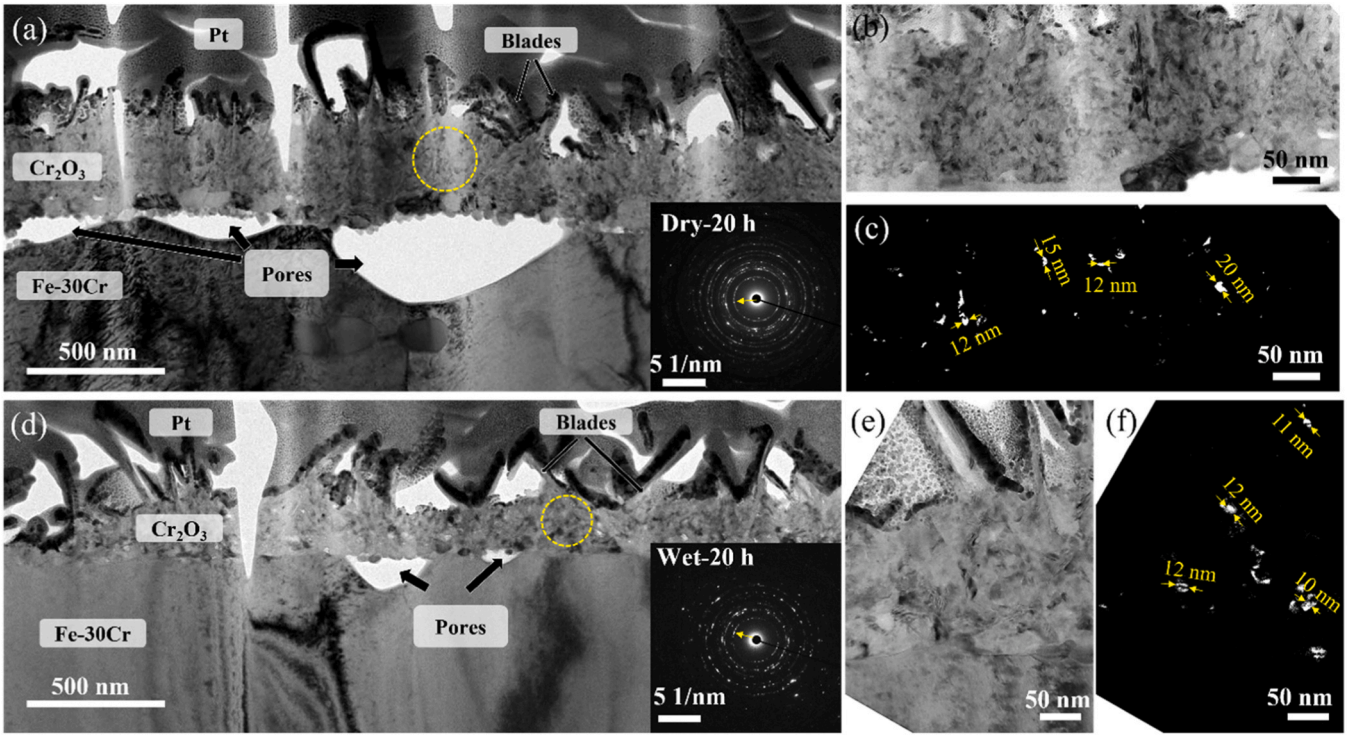

Fig. 3. Fe-30Cr reacted at 650 °C for 20 h in Ar-0.5%SO_2: (a) BF-TEM cross-section and SAD pattern of Cr_2O_3 layer (b) high magnification BF-TEM and (c) high magnification DF-TEM cross-section image of Cr_2O_3 layer in (a); Fe-30Cr reacted at 650 °C for 20 h in Ar-10%H_2O-0.5%SO_2: (d) BF-TEM cross-section and SAD pattern of Cr_2O_3 layer (e) high magnification BF-TEM and (f) high magnification DF-TEM cross-section image of Cr_2O_3 layer in (d). DF images from yellow dash circles, SAD patterns from yellow arrow spot.

alloy interface, with a lateral size of ~250 nm, and depth of ~100 nm measured for the largest one seen. By tilting the beam to select the reflection spot from the Cr_2O_3 rhombohedral {10$\bar{1}$4} plane, the grain size was determined to be 11 ± 1 nm after this exposure (Fig. 3e, f).

3.2.2. Reaction after 100 h

Representative scale surface morphologies on Fe-30Cr in dry and wet SO_2 for 100 h are shown in Fig. 2c and d. The blade-like scale surface morphology was maintained for the longer dry gas exposure, while fine whiskers developed on top of the oxide blades during exposure to wet gas. A TEM cross-section (Fig. 4a) revealed that the scale grown in dry gas had an overall thickness of ~840 nm, with a thickness of ~200 nm for the outer blade zone. A ~ 2 μm long void developed laterally along the scale-oxide interface to a depth of ~300 nm into the alloy. Analysis by SAED (inset of Fig. 4a) again confirmed the scale to be Cr_2O_3 rhombohedral polycrystals.

The scale grown after 100 h in wet gas (Fig. 4d) had an overall thickness of ~1.6 μm, with a ~1.1 μm thick outer blade/whisker zone. Smaller pores with long edges of ~600 nm, ~100 nm in depth were found at the scale-oxide interface. The scale was also identified as Cr_2O_3 by SAED (inset of Fig. 4d). Grain size analysis was performed on the dense oxide layer by dark-field imaging after 100 h reaction in dry gas (Fig. 4b, c) produced slightly larger grains (30 ± 3 nm) than those grown in wet gas (Fig. 4e, f, 20 ± 5 nm).

3.3. Composition of corroded samples

3.3.1. Reaction in dry SO_2

Analysis by STEM/EDX was performed on samples reacted for 20 h (Figs. 5 and 6) and 100 h (Fig. 7) to examine the sulphur ingress. The S-map for the 20 h reaction sample (Fig. 5), shows sulphur accumulation in the oxide layer above the pores at the scale-alloy interface. Point analysis (P1&P2) indicated Cr was depleted to ~9.5 at% near the surface of the underlying alloy. The composition of external Cr_2O_3 scale was confirmed approximately by EDS analysis at P3.

Within the subsurface alloy, partially sulphidised Cr-rich particles 110–150 nm in size are seen in the S-map, adjacent to Cr-rich Fe-Cr particles ~ 200 nm in size that are located near the Cr-depleted region/pristine alloy interface. The compositional profile revealed by line scan analysis (L1) across the left precipitate showed that the S-rich particle had a maximum S concentration of 12.4 at%, and the adjacent Cr-rich precipitate had a maximum Cr concentration of 38.6 at%. The right precipitate (L2) was similar, where the S-rich particle had a maximum S concentration of 19.2 at%, adjacent to a Cr-rich precipitate with a maximum Cr concentration of 61.3 at%.

The iron and chromium EDX maps in Fig. 5 show that the Cr-depleted subsurface region is single-phase and Fe-rich, whereas the parent alloy consists of two finely interspersed Fe- and Cr-rich phases.

Examination of another region of the sample reacted for 20 h in dry gas (Fig. 6) shows a large Cr-rich sulphide bridging the void at the alloy-scale interface together with S-segregation on both the underlying metal surface and the underside of the scale. An internal sulphide also precipitated within the alloy (S-map, L2). EDS (L1) showed that the

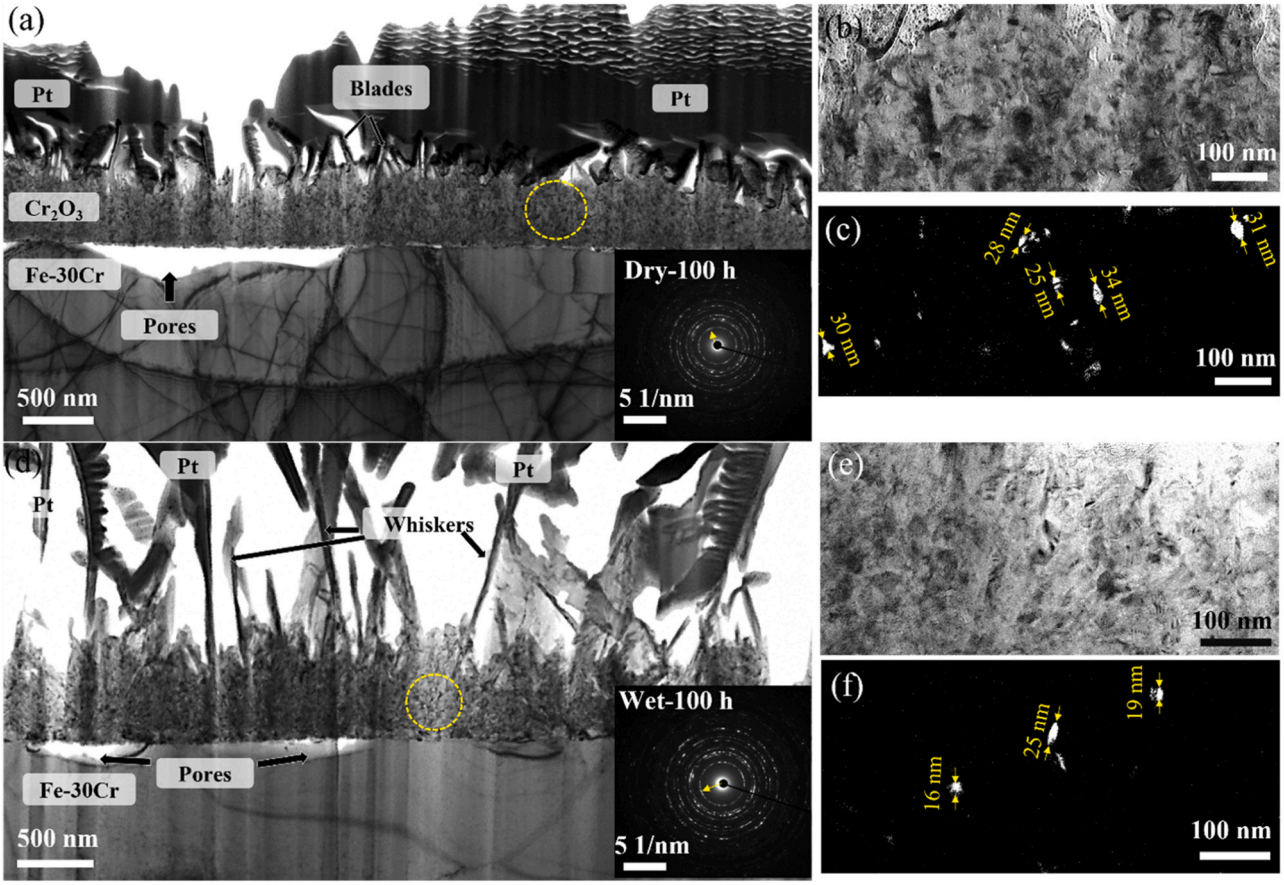

Fig. 4. Fe-30Cr reacted at 650 °C for 100 h in Ar-0.5%SO_2: (a) BF-TEM cross-section and SAD pattern of Cr_2O_3 layer (b) high magnification BF-TEM and (c) high magnification DF-TEM cross-section image of Cr_2O_3 layer in (a); Fe-30Cr reacted at 650 °C for 100 h in Ar-10%H_2O-0.5%SO_2: (d) BF-TEM cross-section and SAD pattern of Cr_2O_3 layer (e) high magnification BF-TEM and (f) high magnification DF-TEM cross-section image of Cr_2O_3 layer in (d). DF images from yellow dash circles, SAD patterns from yellow arrow spot.

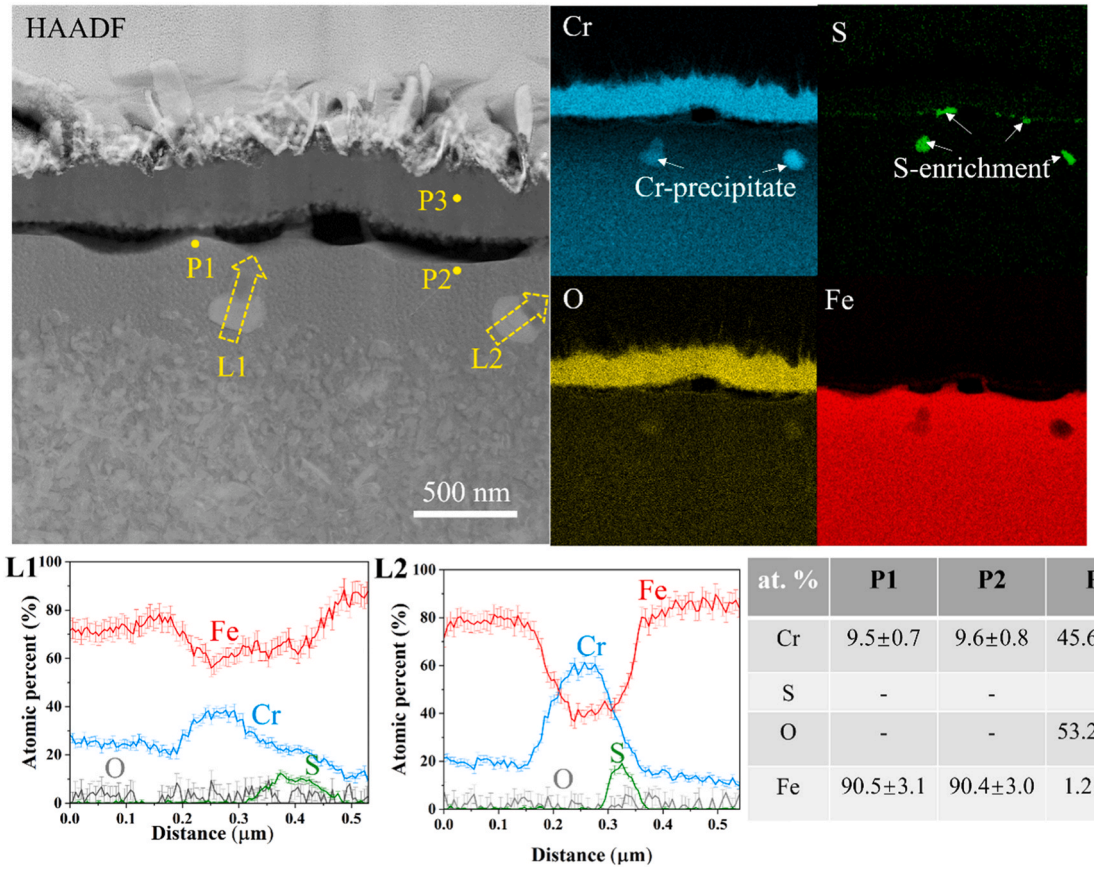

at. %	P1	P2	P3
Cr	9.5±0.7	9.6±0.8	45.6±2.3
S	-	-	-
O	-	-	53.2±3.9
Fe	90.5±3.1	90.4±3.0	1.2±0.1

Fig. 5. Fe-30Cr reacted in Ar-0.5%SO_2 for 20 h: STEM-HAADF image and EDS maps; EDS line profiles; Point analysis.

interfacial sulphide had an average composition of ~43.4 at% Cr and 53.7 at% S, while the internal sulphide (L2) had ~28.2 at% Cr and ~33.5 at% S, both corresponding to a composition of $Cr_{1-x}S$. Sulphide stoichiometries are considered further in the Discussion.

With the increase in exposure time to 100 h, the Cr concentration in the alloy was even more depleted (Fig. 7), leaving ~5.2 at% (P1) in the alloy immediately beneath the scale, and ~6.5 at% (P2) beneath an interfacial pore. Sulphur segregation at the scale-alloy interface initially seen after 20 h (Fig. 5 & 6) was no longer apparent in the S-map (Fig. 7) after 100 h. The external chromia scale remained S-free (P3, P4), and internal Cr-sulphide precipitates were found at deeper sites (up to ~1.6 μm), as seen in the Cr- and S-maps (Fig. 7).

Internal sulphides were located not only at the Cr-depleted region/original alloy interface, but also along a curved boundary as seen in the HAADF image in Fig. 7, which is presumably a grain boundary in the original alloy. The sulphide near the scale-alloy interface (L1) had a maximum S concentration of 41.1 at%, and Cr concentration of 40.5 at %. A precipitate at a deeper site (L2) had a maximum S concentration of 43.3 at%, and Cr concentration of 42.7 at%. Both correspond to $Cr_{1-x}S$. Unlike the 20 h reaction case (Fig. 5), there remained no unreacted Cr-rich metal particle in contact with the sulphide. The dimensions of those sulphides are ~200 nm. In addition, some oxygen enrichment had developed along the alloy surface of the pore, as seen in the O-map and profile L3.

3.3.2. *Reaction in wet SO_2*

STEM/EDX analysis was also carried out on samples reacted with wet gas for 20 h (Figs. 8 and 9) and 100 h (Figs. 10 and 11). After 20 h (Fig. 8), Cr was depleted to 13.9 at% (P1) in the alloy in contact with scale and 10.1 at% (P2) under an interfacial pore. Sulphur was enriched on the underside of the scale facing the pore, as seen in the S-map and line scan analysis (L). The S-rich layer above the scale-pore interface had a composition of ~54.0 at% Cr and 42.7 at% S at P3, suggesting the formation of Cr-sulphides. The external chromia scale was identified by P4. Another region of the sample reacted for 20 h in wet gas (Fig. 9) reveals Cr-sulphides scattered on the underside of the scale, as seen in the line scan analysis and S-map.

With increased exposure time to 100 h, the Cr concentration in the most-depleted alloy region immediately beneath the scale was somewhat lower at ~12.6 at% (P1 &P2 in Fig. 10). In contrast with the dry gas case (Fig. 7, S-map, L), the S-rich layer at the scale-alloy interface was maintained after 100 h reaction in wet gas (Fig. 10, S-map, profile L). Representative compositions in the S-rich layer analysed at P3 showed Cr: 40.1 at%, S: 8.2 at%, and O: 49.7 at%. Another region of this sample (Fig. 11) showed 3 at% sulphur enrichment at the scale-alloy interface according to L1, as well as a Cr-sulphide particle at the scale-alloy interface with a composition of ~40.6 at% Cr and ~54.2 at% S according to L2, close to $Cr_{1-x}S$. No internal sulphides were found within the base alloy for any samples reacted with wet SO_2 in this study.

In summary, the composition of corroded samples under different conditions was examined. In the dry SO_2 reaction, analysis of samples reacted for 20 h revealed sulphur accumulation in the oxide layer at the scale-alloy interface, as well as Cr depletion near the alloy surface. Partially sulphidised Cr-rich particles were observed within the subsurface region of the alloy, alongside Cr-rich Fe-Cr particles. After 100 h, additional sulphide precipitates were found at deeper locations within the alloy substrate, but no sulphur was detected at the scale-alloy interface. These interfacial and internal sulphides were identified as $Cr_{1-x}S$ compounds. Similar trends were observed in the wet SO_2 reaction, with sulphur enrichment, Cr depletion, and the formation of Cr-sulphides at the scale-alloy interface for both 20 and 100 h. However, no internal sulphides were found inside the substrate for wet SO_2 samples, regardless of the duration of the reaction.

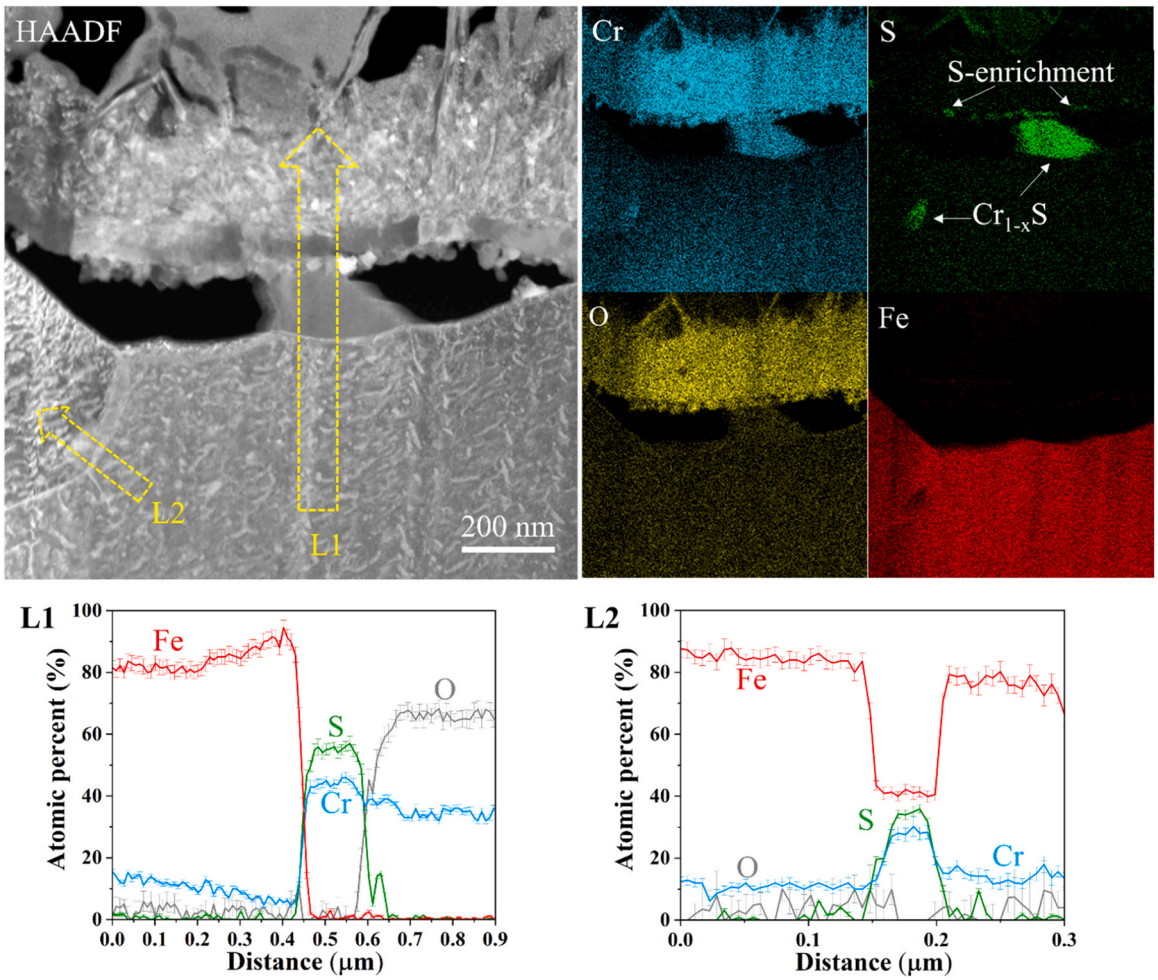

Fig. 6. Fe-30Cr reacted in Ar-0.5%SO_2 for 20 h (another region): STEM-HAADF image and EDS maps; EDS line profiles.

3.4. *Transport of sulphur through Cr_2O_3 scale*

Distributions of sulphur and iron in the Cr_2O_3 layer developed in dry SO_2 after 100 h and wet SO_2 also after100 h were revealed using reconstructed atom maps. The principal ionic species collected by APT were O^+, O_2^+ for oxygen, Cr^+, Cr^{2+}, CrO^+, CrO^{2+}, CrO_2^+, CrO_2^{2+}, CrO_3^+ for chromium, Fe^+, Fe^{2+}, FeO^+, Fe_3O^+ for iron, and SO^+, SO^{2+}, SO_2^+ for sulphur. Fig. 12 shows three-dimensional atom maps in which ~20 nm thick slices through the data have been visualised, parallel to the tip axis. Fig. 12a, for the dry gas reaction, reveals that sulphur and iron species are mostly distributed in the same locations, along curved boundaries. In contrast, Fig. 12d, for the wet gas reaction, shows that Fe is located alongside the boundaries on which sulphur is segregated.

The scale was made up of chromia grains revealed by TEM (Fig. 4c, f) to be ~16–25 nm in size, consistent with the sulphur enriched boundaries observed in the APT S-maps. Bulk compositional analysis showed a total of 0.10 at% S in the oxide scale grown in dry SO_2, compared with 0.15 at% S in the wet SO_2 case.

Proximity histograms were used to measure the composition profile around the grain boundaries. S isoconcentration surfaces were used to define regions near the grain boundaries and the proximity histogram shows the variation of composition moving away from a selected S-rich oxide grain boundary. In the scale grown in dry SO_2 for 100 h the location is indicated by an arrow in Fig. 12a, S-map. As shown in Fig. 12b, a threshold sulphur level of 0.8 at% (at the position marked zero) served to locate the grain boundary. The maximum sulphur concentration at the grain boundaries according to Fig. 12b is 1.8 ± 0.07 at %. As for the Fe concentration across the S-grain boundary plotted in Fig. 12b, a slightly higher value is found in the grain boundary than in the grain interior.

Grain interiors were examined by analysing volumes with sulphur concentrations below 0.1 at%, yielding an average sulphur concentration of 0.03 ± 0.02 at%. The grain boundary segregation factor of sulphur was in this way calculated to be ~60.

Fe-containing ions were also detected in higher amounts at the curved grain boundaries. The 3.0 at% Fe iso-surface was used at the position marked zero (Fig. 12c) for the dry gas reaction as a threshold to locate the Fe-rich zone. The proximity histogram in Fig. 12c demonstrates a maximum Fe concentration of 4.9 ± 0.17 at% at a distance of 0.3 nm from a selected boundary (arrowed in the Fe-map of Fig. 12a). The average iron concentration within the grain interiors with iron concentrations below 0.5 at% was calculated to be 0.4 ± 0.05 at%. Thus the segregation factor for iron was calculated to be ~12 in the dry gas case. Similarly, the sulphur concentration is higher in the Fe-rich boundary than in the Fe-poor grain (Fig. 12c).

In the wet gas reacted sample, which has a higher overall sulphur concentration, sulphur-rich grain boundaries are again seen in the S-map of Fig. 12d. As shown in Fig. 12e, a threshold sulphur level of 1.6 at % was used (at the position marked zero) to define the enrichment location and the maximum concentration was found to be 3.1 ± 0.13 at %. The average sulphur concentration in the grain interiors was measured to be 0.04 ± 0.03 at%, and thus a segregation factor of ~78 was calculated.

In contrast with the sample grown in dry gas, iron segregated into the adjacent grains, rather than at the S-rich grain boundaries (Fig. 12d, Fe-map). A proximity histogram of an Fe-rich region adjacent to a grain

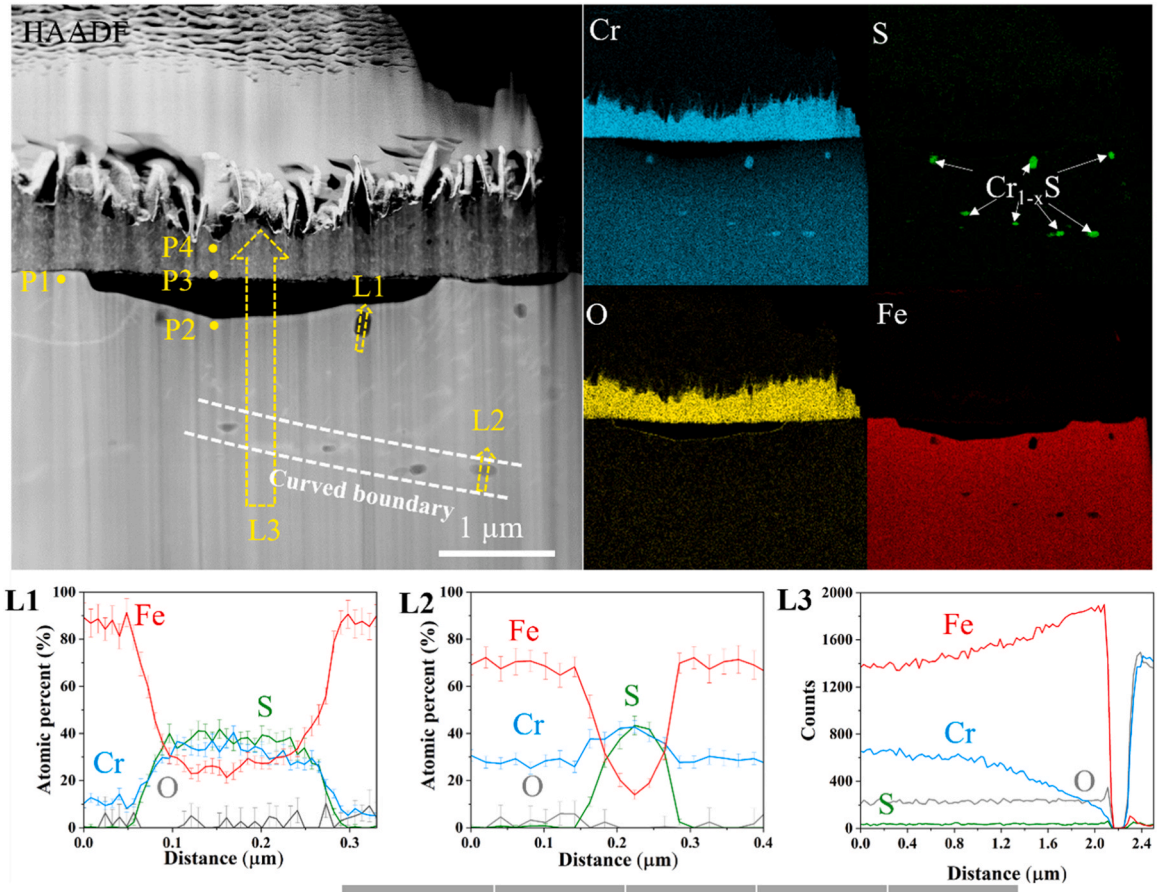

at. %	P1	P2	P3	P4
Cr	5.2±0.3	6.5±0.4	35.5±2.3	36.8±2.5
S	-	-	-	-
O	-	-	62.6±4.6	62.5±5.1
Fe	94.8±3.6	93.5±2.9	1.9±0.1	0.7±0.2

Fig. 7. Fe-30Cr reacted in Ar-0.5%SO_2 for 100 h: STEM-HAADF image and EDS maps; EDS line profiles; Point analysis.

boundary (location indicated by an arrow in Fig. 12d, Fe-map) as shown in Fig. 12f showed its composition at a distance of 2.6 nm from the 4.5 at % Fe iso-surface is 13.1 ± 1.4 at% Fe, ~32.1 ± 1.9 at% Cr, ~54.5 ± 2.1 at% O, corresponding to the (Cr, Fe)$_3O_4$ spinel phase.

In general, Cr_2O_3 scales formed in wet SO_2 gas contained a higher bulk sulphur concentration as well as higher levels of grain boundary segregation than those grown in dry SO_2 gas. Iron tends to accumulate in grain boundaries the way sulphur does in the dry grown oxide, but segregates to regions parallel to grain boundaries in oxide grown in wet gas. The uptake of sulphur by the chromia scale is enhanced when water vapour is present. It is to be noted that any H-bearing species in the sample originating from the reaction gas would not be detected since a large fraction of any such species would be lost during sample preparation by FIB milling.

3.5. *Two-stage corrosion experiment*

A two-stage corrosion experiment (Ar-10%H_2O for 20 h then Ar-0.5%SO_2 for 20 h) was carried out to investigate the possibility of sulphur ingress into a preformed Cr_2O_3 scale. A TEM cross-section (Fig. 13a) shows the Cr_2O_3 scale preformed in a single-stage experiment had an average thickness of ~100 nm and consisted of relatively equiaxed grains of variable dimensions, ranging from ~15–40 nm.

The scale on an alloy subjected to the two-stage experiment (Fig. 13b) demonstrated a duplex structure: an inner Cr_2O_3 layer with an average thickness of ~40 nm, and an outer Cr_2O_3 scale with an average thickness of ~ 100 nm. The inner Cr_2O_3 scale consisted of elongated grains with grain size of ~40 to ~60 nm, while the outer layer had much finer grains of ~20–30 nm. STEM/EDX analysis (Fig. 13c) revealed no sulphur segregation at any interface, nor internal sulphidation within the alloy.

The outer layer resulting from the two-stage reaction corresponds approximately in thickness, and broadly in grain size, to the single layer formed in the first-stage pre-oxidation reaction. In this case, the second reaction stage produced slightly coarser-grained oxide beneath the preformed layer, reflecting inward oxidant diffusion.

4. Discussion

Corroded Fe-30Cr alloys exposed in dry and/or wet SO_2 gases at 650 °C were investigated. It was found that oxidation and sulphidation developed differently with exposure time in the two gases.

An external chromia scale was the principal product under all gas conditions examined. The main features of the corrosion products developed in dry and wet SO_2 gases are summarised in Table 2. As is seen, the dense chromia scale layer grew more slowly in wet gas than in

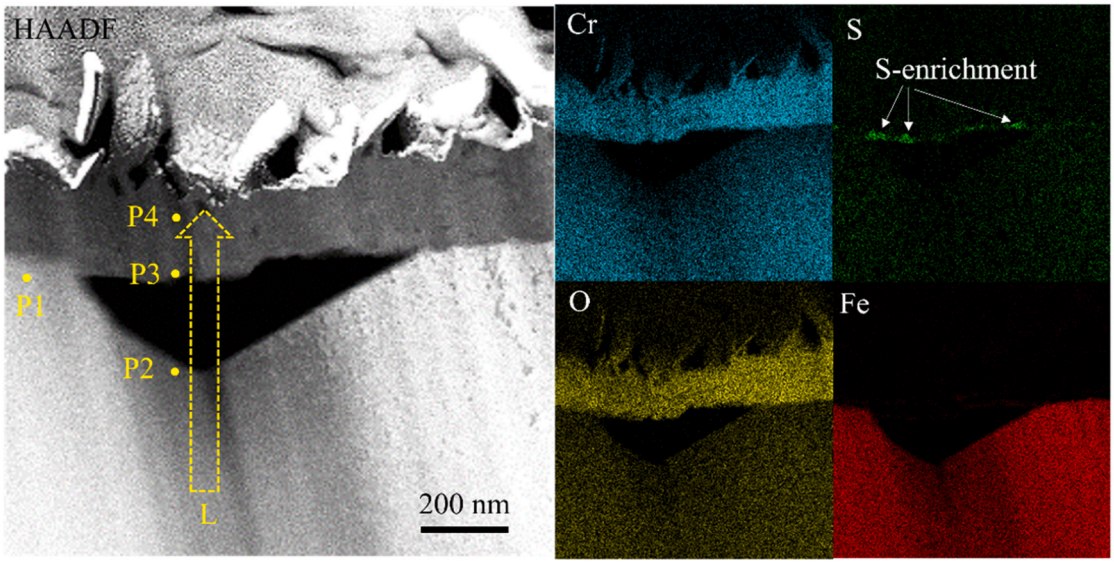

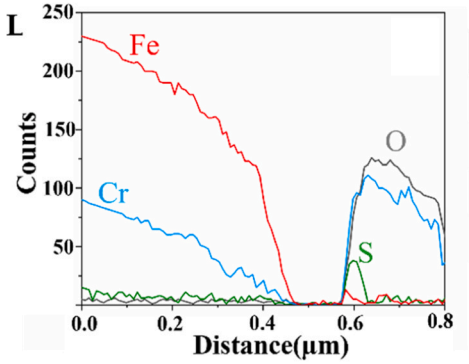

at. %	P1	P2	P3	P4
Cr	13.9±1.1	10.1±1.0	54.0±3.9	34.1±2.2
S	-	-	42.7±2.8	-
O	-	-	1.4±0.5	64.7±5.1
Fe	86.1±4.5	89.9±4.7	1.9±0.3	1.2±0.1

Fig. 8. Fe-30Cr reacted in Ar-10%H_2O-0.5%SO_2 for 20 h: STEM-HAADF image and EDS maps; EDS line profiles; Point analysis.

dry SO_2. Conversely, the outer chromia blade zone extended more rapidly in wet SO_2 than in dry gas. Different degrees of sulphur uptake are also seen from a comparison of wet and dry gas results.

Internal sulphidation resulted from exposure to dry SO_2, but was not observed after reaction with wet gas. Despite this difference, sulphur was in most cases found segregated to the scale-alloy interface: in dry gas after 20 h (Figs. 5 and 6), and in wet gas after both 20 (Figs. 8 and 9) and 100 h exposure (Figs. 10 and 11). Close examination of the profile L3 in Fig. 7 reveals slight S-enrichment at the underside of the scale above a large interfacial void. However, the corresponding experiment in wet gas yielded more interfacial S-segregation (Figs. 10 and 11), sufficient to form a distinct chromium sulphide particle.

Evidently, a complex interaction between the different oxidants, SO_2 and water vapour, effects both oxidation and sulphidation of this Fe-30Cr alloy. The following discussion goes first to thermodynamic and kinetic analyses of this process, and then focuses on the interaction of SO_2 with growth of protective Cr_2O_3 scales and the role of H_2O in this interaction.

4.1. Thermodynamic considerations

Since no Fe-rich oxides or sulphides were found, a predominance phase diagram of the Cr-O-S system, as shown in Fig. 14, was used to simplify the thermodynamic phase stability analysis. Points A and D represent the gas phase conditions at the scale surface in dry and wet SO_2 gas, respectively, and are seen to lie in the Cr_2O_3 field. This oxide is therefore predicted to form at the scale surface, as was observed.

Although the FactSage database yields a thermochemical diagram for Cr-S-O (Fig. 14) showing a Cr_5S_6 phase field, the existence of this phase at reaction temperature is doubtful. Indeed, $Cr_{1-x}S$ has been shown to be stable at 700 °C [18]. When cooled to room temperature, $Cr_{1-x}S$ decomposes into a series of phases which include Cr_5S_6. The high temperature leads to the formation of $Cr_{1-x}S$ (x varies from 0.02 to 0.2).

The sulphur partial pressure in dry SO_2 (2.8×10^{-11} atm) is sufficient to sulphidise Cr, while that in wet SO_2 (1.4×10^{-17} atm) is not. However, the oxygen partial pressure is kept to a low value at the scale-alloy interface by the metal-oxide equilibrium, and might therefore lead to an elevated sulphur partial pressure through the equilibrium:

$$SO_2(g) = O_2(g) + \frac{1}{2}S_2(g), \Delta G^o = 294.4\text{kJ} \quad (1)$$

The SO_2 isobar for an SO_2 level of 0.005 atm is plotted on the diagram as a grey dashed line. The relationship between sulphur and oxygen partial pressures on the SO_2 isobar is defined by Eq. (1).

Since a chromia scale formed on the alloy in both gas conditions, the p_{O_2eq} at the scale-alloy interface during the initial stage of oxidation is assumed to be determined by the equilibrium between Cr_2O_3 and Cr dissolved in the ferritic matrix:

$$2Cr(s) + \frac{3}{2}O_2(g) = Cr_2O_3(s), \Delta G^o = -886.2\text{kJ} \quad (2)$$

Approximating $a_{Cr} = 0.3$, the corresponding p_{O_2} value at the scale-alloy interface is calculated to be 1.9×10^{-33} atm. Due to limited SO_2 transport through the thickening chromia scale, its partial pressure is < 0.005 atm, and the equilibrium values of p_{S_2} are less than those on the SO_2 isobar. The situation is represented schematically by diffusion paths such as A-B for dry SO_2, and D-E for wet SO_2.

The oxygen and sulphur potentials are expected then to follow the CrS/Cr_2O_3 phase boundary to a point such as F, where the underlying

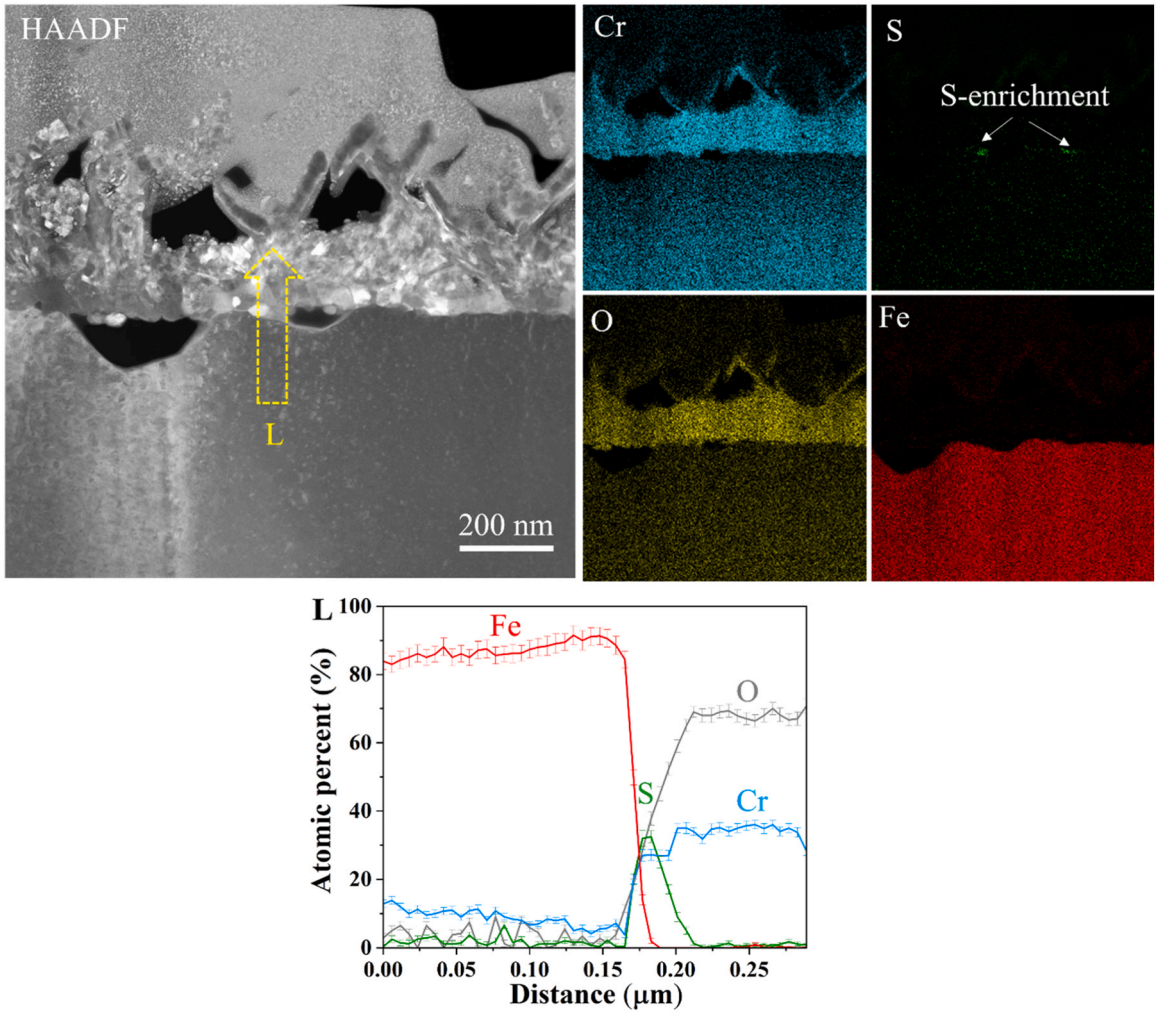

Fig. 9. Fe-30Cr reacted in Ar-10%H_2O-0.5%SO_2 for 20 h (another region): STEM-HAADF image and EDS maps; EDS line profiles; Point analysis.

alloy is in contact with the oxide-sulphide scale. Internal sulphides formed within the base alloy in dry SO_2, which is represented by a point such as C. Thus the observed phase assemblages are in accord with local equilibrium throughout the reaction zone. The absence of internal sulphides in wet SO_2 reaction products is discussed below.

4.2. Transport of SO_2 through Cr_2O_3 scale

The observation of internal $Cr_{1-x}S$ precipitates beneath a chromia scale on ferritic alloys has been frequently reported and have only been observed after oxide scales had formed [19–23]. Thus, oxidation takes place prior to sulphidation of alloys in SO_2, and sulphur must penetrate the Cr_2O_3 scale.

The formation of Cr_2O_3 scale relies on grain boundary diffusion of chromium and/or oxygen within the oxide [24–26]. Atom probe analysis of the chromia scale formed in both dry and wet SO_2 gases (Fig. 12, S-maps) identified sulphur along oxide grain boundaries. It is thusly confirmed that both sulphur and oxygen, presumably in the forms of SO_2 and/or S_2, penetrated along Cr_2O_3 grain boundaries, during reaction with SO_2.

Sulphur uptake in most cases manifested in the form of sulphur segregation and/or $Cr_{1-x}S$ particles at the scale-alloy interface (Figs. 5,6 and 8–11), whose concentrations depended on the amount of sulphur transported through the oxide, and was directly affected by the presence of H_2O in the gas. Before discussing those effects, early stage oxidation and sulphidation are considered briefly.

4.2.1. Oxidation and sulphidation in dry SO_2

The amount of sulphur and/or $Cr_{1-x}S$ (Figs. 5 and 6) segregated beneath the Cr_2O_3 scale after 20 h exposure to dry SO_2 gas is rather small, suggesting competing processes of sulphide formation and destruction may take place.

Possible reactions at the scale surface in SO_2 gas include [27]:

$$2Cr(s) + \frac{3}{2}SO_2(g) = Cr_2O_3(s) + \frac{3}{4}S_2(g), \Delta G^o = -444.6kJ \quad (3)$$

$$\frac{7}{2}Cr(s) + \frac{3}{2}SO_2(g) = \frac{3}{2}CrS(s) + Cr_2O_3(s), \Delta G^o = -738.9kJ \quad (4)$$

$$2CrS(s) + \frac{3}{2}SO_2(g) = Cr_2O_3(s) + \frac{7}{4}S_2(g), \Delta G^o = -173.4kJ \quad (5)$$

In this description, the sulphur enrichment and $Cr_{1-x}S$ particles (Figs. 5 and 6) detected at the scale-alloy interface are attributed to reactions (3) and (4), respectively, where simultaneous formation of oxides and sulphides and/or sulphur adsorption took place in the early reaction stages, as has been suggested previously [19,28–30].

Alternatively, it has been proposed that SO_2 enters the oxide scale and penetrates to the oxide interface [31]. At this interface, the oxygen activity is low, controlled by the Cr/Cr_2O_3 equilibrium. As a result, the sulphur activity is increased via reaction (1), and CrS formation by reaction (3) is promoted.

Barely any sulphur remained at the scale-alloy interface after 100 h exposure to dry gas (Fig. 7) compared to that in the 20 h experiment

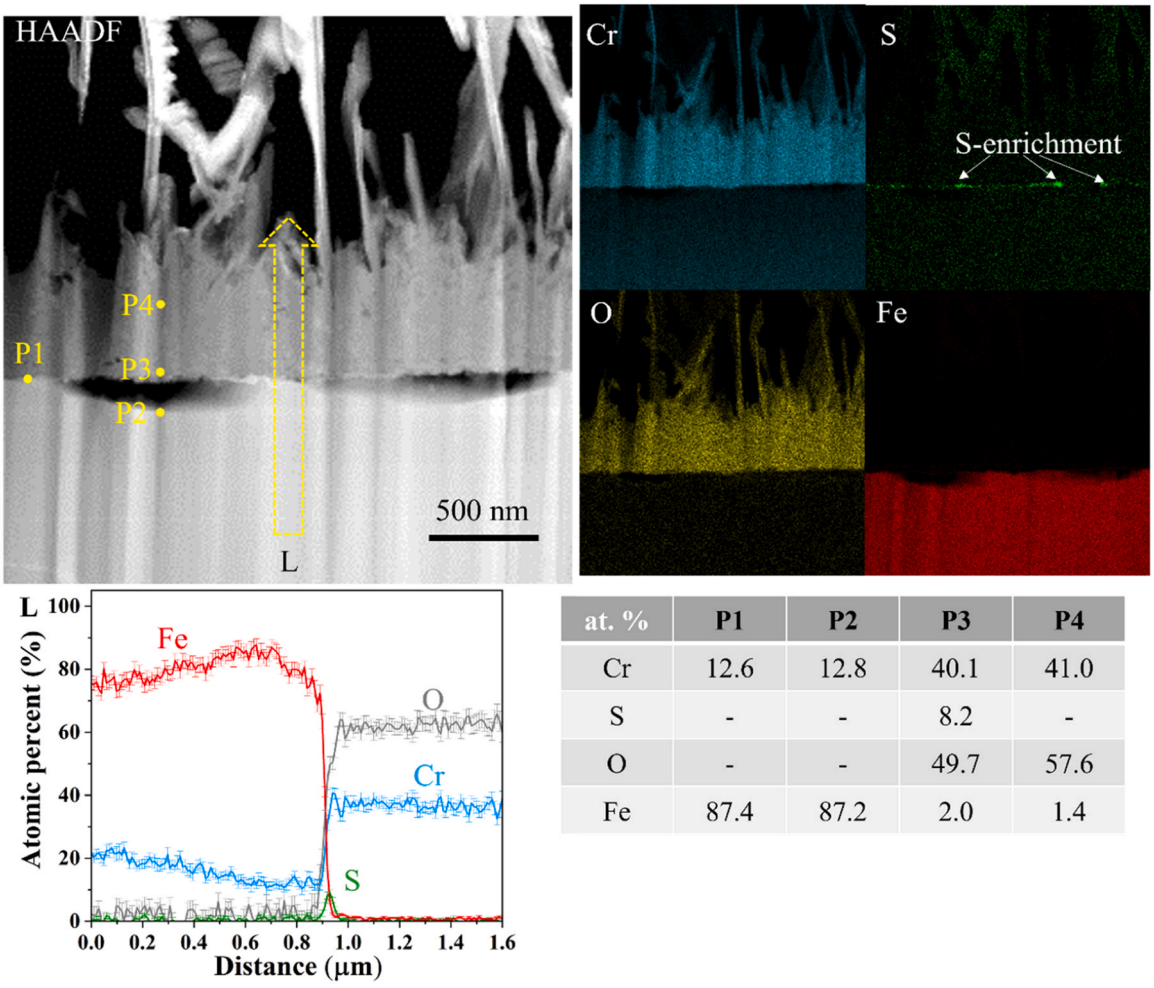

at. %	P1	P2	P3	P4
Cr	12.6	12.8	40.1	41.0
S	-	-	8.2	-
O	-	-	49.7	57.6
Fe	87.4	87.2	2.0	1.4

Fig. 10. Fe-30Cr reacted in Ar-10%H_2O-0.5%SO_2 for 100 h: STEM-HAADF image and EDS maps; EDS line profiles; Point analysis.

(Figs. 5 and 6). Thus, oxidation of the initially formed sulphides via reaction (5) is indicated, favoured by the greater oxide stability and continued SO_2 supply because of the continuous flow of SO_2 in the gas system and relatively fast internal diffusion via chromia grain boundaries. The released sulphur tends to be driven further inward, forming internal $Cr_{1-x}S$ precipitates, instead of escaping outwards, as also observed by Choi and Stringer [32]. This accounts for the observation that the number and depth of internal $Cr_{1-x}S$ precipitates increased with reaction time in dry SO_2 gas (Fig. 7, S-maps).

4.2.2. *Sulphur transport through Cr_2O_3 scale in dry SO_2*

Sulphide oxidation could also produce pores within the newly formed chromia. The volume per unit mole of Cr in $Cr_{1-x}S$ (CrS: 17.19 cm^3) is larger than that in the oxide (Cr_2O_3: 14.56 cm^3), facilitating gas species access to the reaction front. However, neither cracks nor pores were observed within the chromia scale, possibly because of inward transport of oxidants to grow more oxide at the scale-alloy interface, filling any free space created.

Due to the limited inward transport of molecular gas species such as SO_2, the sulphide oxidation reaction beneath the scale could also be:

$$2CrS(s) + \frac{3}{2}O_2 = Cr_2O_3(s) + S_2, \Delta G^o = -615kJ \quad (6)$$

Clearly the continued sulphur enrichment and/or $Cr_{1-x}S$ particle stability rests with the relative amounts of oxygen and/or sulphur transport through the oxide. With scale thickening, the inward transport of both oxidant species is slowed, and the equilibrium state of (6) can in this way be affected.

In order to reach the scale-alloy interface, sulphur species make use of diffusion sites on oxide grain boundaries. The presence of strongly adsorbed sulphur on diffusion sites in oxide grain boundaries could in principle reduce the ingress of oxygen, which would otherwise oxidise the sulphides. However, the opposite effect was observed in the current study: the ratio of sulphur to oxygen ingress was insufficient to sustain the stability of the initially formed sulphides found beneath the chromia scale (Table 2, Fig. 7).

In the two-stage experiment (Fig. 13), no SO_2 was present in the initial stages of reaction, and no sulphur was incorporated into the first-formed scale. When that pure oxide scale was exposed to SO_2, oxygen penetrated the initial oxide, but sulphur did not. This confirms that for this high chromium alloy, sulphur is incorporated into its oxide scale only during initial exposure of metal to an SO_2 containing gas. Once an oxide scale is well established, no sulphur penetration occurs.

4.2.3. *Oxidation and sulphidation in wet SO_2*

The presence of water vapour in SO_2 gas introduces an additional and more abundant oxidant and alters the corrosion behaviour. Nonetheless, reaction by SO_2 remains evident close to the scale-alloy interface. The growth of chromia whiskers observed in an atmosphere containing steam with negligible free oxygen, but not seen in a dry, oxygen-bearing atmosphere has been well documented [33–35].

Despite significant thickening of the total external oxide (~1.6 μm) in wet gas after 100 h in comparison with that in dry gas (~840 nm), the weight uptake was reduced (~0.085 mg/cm^2 in wet gas compared with ~0.113 mg/cm^2 in dry gas). This is because of the extremely low

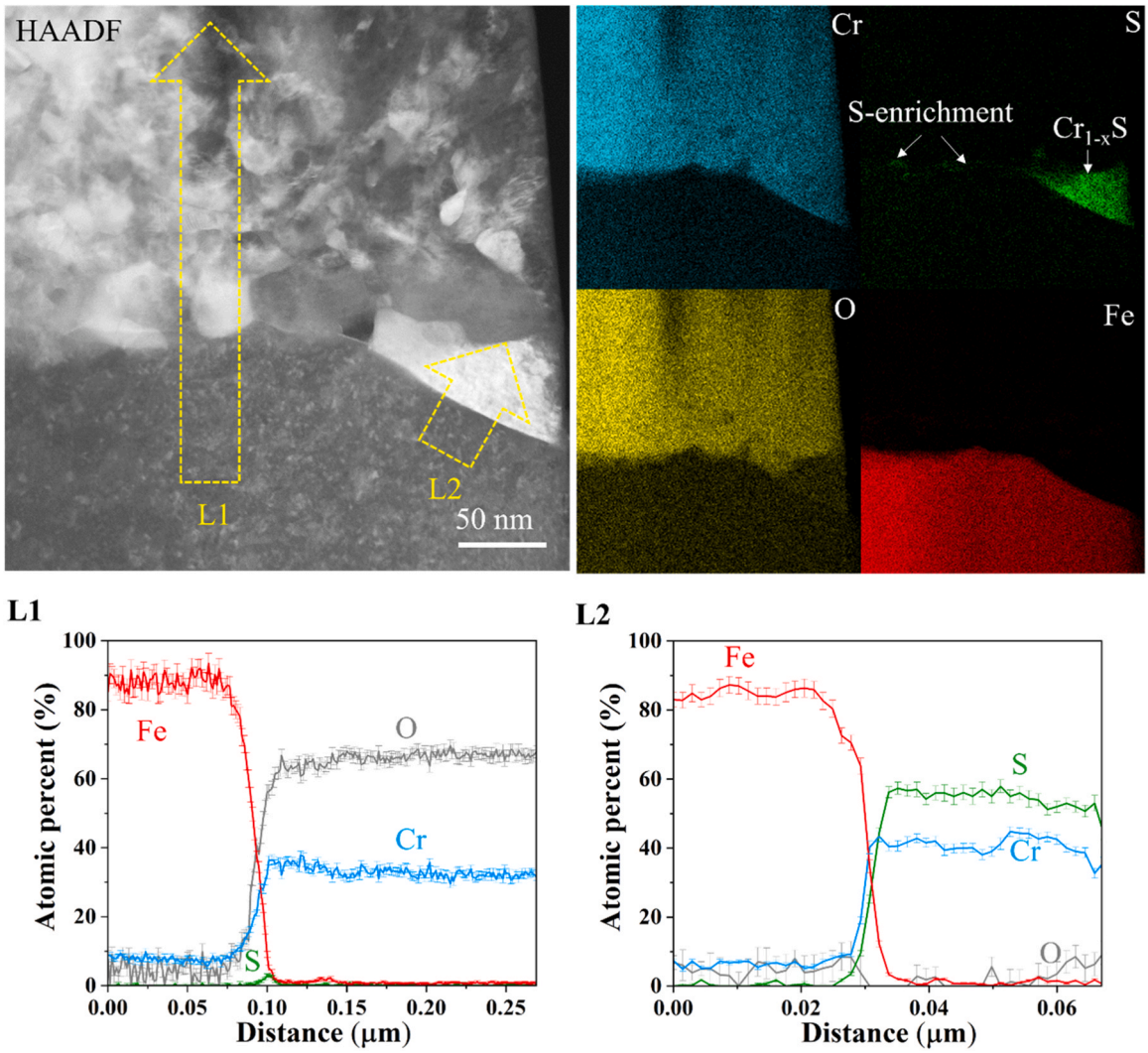

Fig. 11. Fe-30Cr reacted in Ar-10%H_2O-0.5%SO_2 for 100 h (another region): STEM-HAADF image and EDS maps; EDS line profiles; Point analysis.

volume fraction of solid contributed by the sparse oxide whiskers compared with the density of the compact underlying oxide layer, the latter being predominant in the measured weight uptake. The underlying oxide layer has a higher average thickness after 100 h in dry gas (~640 nm) than for wet gas (~500 nm). Approximating the oxide as pure Cr_2O_3, the weight gain due to the dense layer is calculated to be ~0.106 mg/cm^2 for the dry gas reaction, and ~0.083 mg/cm^2 for wet gas, accounting for nearly all the weight gain in each case.

Quantification of the sulphide reaction products for the reacted samples from TEM analysis was unsatisfactory due to the limited region examined. A qualitative comparison is available from previous work. By exposing Fe-20Cr to Ar-20%CO_2-0.5%SO_2 gases at 650 °C for 10 min, Yu et al. [36] found from XPS measurements that the amount of $Cr_{1-x}S$ at the scale-alloy interface was lower when 20%H_2O was added to the gas. It was concluded that the reduction in sulphur uptake was associated with H_2O-derived species on oxide grain boundaries [36]. Such a conclusion, however, does not apply to long-term exposure, as found in this study: $Cr_{1-x}S$ remained at the scale-alloy interface after 100 h exposure to wet SO_2 gas (Figs. 10, 11) but disappeared in dry SO_2 gas (Fig. 7).

In dry SO_2, sulphur was released in the long term by oxidation of sulphide particles and/or adsorbed sulphur at the scale-alloy interface diffused into the alloy to form internal $Cr_{1-x}S$, whereas both forms of sulphur species were found to remain at the interface after 100 h exposure to wet SO_2 gas, and no visible internal sulphides formed. Clearly, a relatively high sulphur activity was maintained at the scale-alloy interface in the latter case. This could only occur if sufficient sulphur penetrated the oxide as a continuing uptake process, promoting the reverse reaction (6).

4.2.4. *Sulphur transport through Cr_2O_3 scale in wet SO_2*

Atom probe analysis showed a higher sulphur uptake in the chromia scale formed in wet gas than in dry gas, as evidenced by the bulk concentration throughout the oxide and segregated concentration along the oxide grain boundaries, as summarised in Table 2. The effect of H_2O in enhancing sulphur uptake in Cr_2O_3 scale is now considered. Inward diffusion of oxygen in growing chromia scales is promoted by H_2O-containing atmospheres, thought to be via rapid diffusion of OH^- [37]. The possibility that transport of other oxidant species such as sulphur is also increased is now considered.

It is thought that H_2O-derived species adsorbed at the grain boundaries tend to slow boundary motion, as reflected by the observed oxide grain refinement [38]. It is reasonable then to propose that the diffusion of other species within the modified grain boundaries could also be altered. Mutual repulsion between polar species such as OH is suggested to result in more disordered boundaries [39]. It is now proposed that such a change in structure could enhance the mobility of grain boundary sulphur.

The presence of H_2O is expected also to affect the diffusion mode of cationic species such as Fe (Fig. 12). In the dry gas grown chromia, Fe

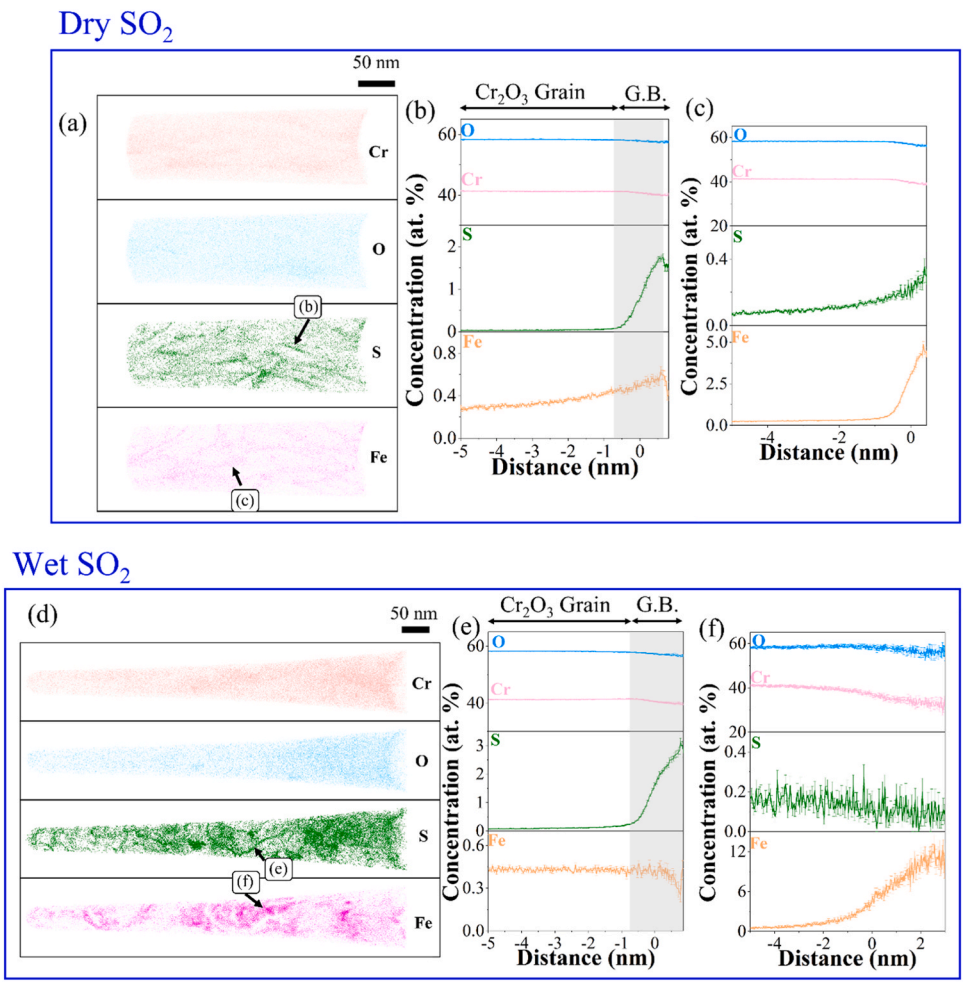

Fig. 12. Fe-30Cr reacted in Ar-0.5%SO_2 for 100 h: (a) atom maps of axial slices through Cr_2O_3 tip; (b) proxigram of species with respect to the 0.8 at% S isoconcentration surface from the area indicated by an arrow in (a) S-map; (c) proxigram of species with respect to the 3.0 at% Fe isoconcentration surface from the area indicated by an arrow in (a) Fe-map; Fe-30Cr reacted in Ar-10%H_2O-0.5%SO_2 for 100 h: (d) atom maps of axial slices through Cr_2O_3 tip; (e) proxigram of species with respect to the 1.6 at% S isoconcentration surface from the area indicated by an arrow in (d) S-map; (f) proxigram of species with respect to the 4.5 at% Fe isoconcentration surface from the area indicated by an arrow in (d) Fe-map.

diffused out predominantly via grain boundaries, and might interfere with sulphur uptake. In contrast, Fe dissolved in the wet gas grown chromia to form spinel in grain interiors rather than segregating along the boundaries. Thus there is no reason to believe the inward sulphur diffusion would be hindered by iron in the wet gas.

Further computational analysis, such as by DFT calculations, is required to predict the stability of iron and/or sulphur at Cr_2O_3 grain boundary sites with and without the incorporation of H_2O-derived species. For the moment, the nano-scale observations explain why accumulation of iron near the grain boundaries allows continued sulphur penetration and the preservation of sulphur and/or sulphides beneath the chromia scale.

4.3. *Effect of H_2O on internal sulphidation*

As is discussed, the presence of H_2O enhanced the inward transport of the oxidant species, leading to a higher level of sulphur uptake in the oxide grain boundaries and at the scale-alloy interface. However, this effect ceased at the scale-alloy interface since no internal sulphides were formed in any wet gas corroded specimens. The reason for this is now considered.

First, it is known that internal sulphidation preferentially occurred at locations with high Cr concentrations, as evidenced by the partial sulphidation on Cr-rich particles within the alloy after 20 h exposure to dry SO_2 (Fig. 5). However, no such Cr-rich particles were found in wet gas exposed samples. To investigate the possibility of any H_2O/H_2 effect on the development of the Cr-rich phase, additional annealing experiments in Ar and Ar-10%H_2 gases at 650 °C for 100 h were performed on uncorroded Fe-30Cr alloy samples. Annealed samples were prepared by FIB milling, and STEM/EDS analysis led to the results shown in Fig. 15.

As seen in the left image in Fig. 15, a small fraction of the alloy near the surface decomposed into heterogenous microstructures consisting of Cr-rich and Cr-poor regions under Ar gas annealing. Quantification by point analysis at P1 indicates an average alloy composition of 32.7 at% Cr and 67.3 at% Fe, which corresponds to Fe-31.2 wt% Cr. Point analysis of Cr-rich regions (P2, P3) showed a normalised concentration of Cr: 44.6 at%, and Fe: 55.4 at%, in line with the composition of σ-phase in the Fe-Cr system [40,41], while the Cr-poor region (P4, P5) showed a normalised composition of Cr: 19.9 at%, and Fe of 80.1 at%.

Decomposition of Fe-30Cr into a 2-phase (α + σ) mixture is to be expected from the binary phase diagram [40,41] at 650 °C. The finely divided microstructure seen in Fig. 15 is typical of spinodal decomposition. As is clear from the annealing experiment, oxidation is not required to derive from alloy phase transformation. However, when oxidation accompanies heat treatment, Cr depletion in the subsurface alloy region causes the Cr-rich σ-phase to dissolve.

In contrast, a homogenous structure was maintained throughout the alloy after Ar-10%H_2 annealing, as no Cr-rich phase was observed (right image in Fig. 15). An average alloy composition of 33.4 at% Cr and 66.6 at% Fe detected corresponds to Fe-31.8 wt% Cr. Evidently, the presence of hydrogen tends to suppress Cr-rich σ-phase formation at 650 °C, which would otherwise contribute to the development of Cr-rich particles as seen in alloys exposed to dry gases, and thus internal sulphidation. Reasons for this effect are uncertain and further investigation is required.

Another possible role of H_2O in suppressing internal sulphidation

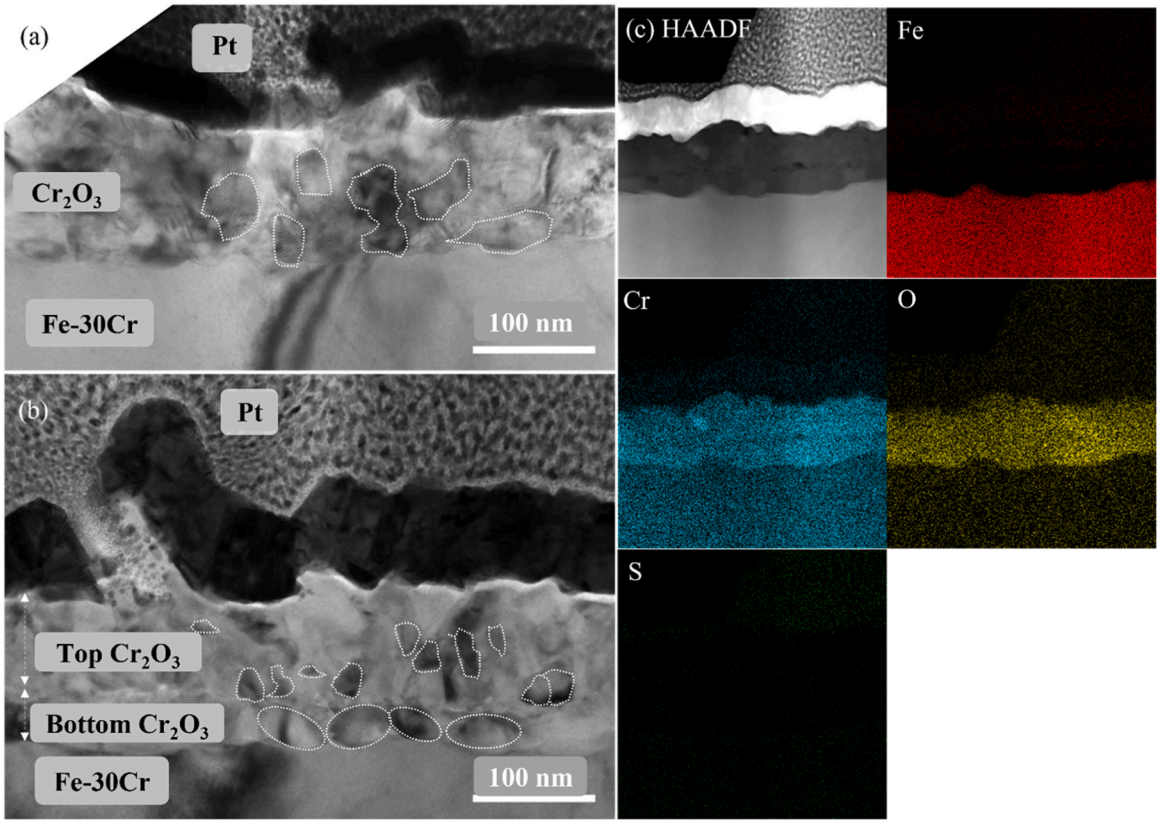

Fig. 13. Fe-30Cr reacted in one-stage experiment (Ar-10%H_2O for 20 h): (a) BF-TEM cross-section of Cr_2O_3 layer; Fe-30Cr reacted in two-stage experiment (Ar-10% H_2O-20 h then Ar-0.5%SO_2-20 h): (b) BF-TEM cross-section of two Cr_2O_3 layers; (c) HAADF image and EDS maps of two-stage corroded alloys.

Table 2
Corrosion product summary for Fe-30Cr alloy in dry and wet SO_2 gas at 650 °C, 1 atm.

Reaction Products	Dry-20 h	Dry-100 h	Wet-20 h	Wet-100 h
Cr_2O_3 blades/ dense layer (nm)	180/270	200/640	200/140	1100/500
Interfacial scale above alloy	$Cr_{1-x}S$/Cr_2O_3	Cr_2O_3	$Cr_{1-x}S$/Cr_2O_3	$Cr_{1-x}S$/Cr_2O_3
Internal precipitates	$Cr_{1-x}S$	$Cr_{1-x}S$	None	None
Internal sulphidation depth (nm)	600	1700	NA	NA
Bulk sulphur concentration (at%) in Cr_2O_3	Unknown	0.10	Unknown	0.15
Average sulphur in Cr_2O_3 grain interior (at%)		0.03 ± 0.02		0.04 ± 0.03
Maximum sulphur in Cr_2O_3 grain boundaries (at%)		1.8 ± 0.07		3.1 ± 0.13
Average iron in Cr_2O_3 grain interior (at%)		0.4 ± 0.05		NA
Maximum iron in Cr_2O_3 grain boundaries (at%)		4.9 ± 0.17		NA

could from its interaction with H_2O-derived species within and beneath the scale. Sulphur segregation at the scale-alloy interface was shown to occur on the free metal surface upon void formation beneath the scale, stabilising the voids or cavities by reducing the surface energy [42]. Instead, sulphur segregation in this study was found within the oxide layer and on its underside above the interfacial cavities (Figs. 8–11).

It is suggested that H_2O-derived species might attach to $Cr_{1-x}S$ particles via OH-S bonding such that dissociation $Cr_{1-x}S$ and thus release of sulphur would be inhibited. It is known [41] that OH-S bonding occurs in liquid solvents, but no information is available for the present situation. Whether or not direct bonding occurs between the secondary oxidant species within a chromia scale remains unknown.

5. Conclusion

Exposure of a chromia-forming alloy to SO_2, with and without the simultaneous presence of H_2O(g), produces a chromia scale as the principal reaction product. However, the degree of protection afforded this scale is affected by the presence within it of sulphur.

This phenomenon can be understood from a recognition that mass transport in chromia scales occurs via grain boundaries, lattice diffusion being negligible. Insight into the complex interactions between sulphur and water vapour-derived species in the scale is also available in this way.

Sulphur within the scales is located overwhelmingly at grain boundaries, as seen in reconstructed atom probe images. These boundaries provide continuous pathways through the scale in the early stages of reaction.

Oxygen activity within the scale decreases with depth beneath the surface, reaching a minimum at the oxide-scale interface. This allows formation of $Cr_{1-x}S$, as a result of the sulphur penetration.

In the absence of H_2O(g), sulphur enrichment at the scale-alloy interface decreases with time as a result of (a) decreased inward S diffusion, plus (b) S diffusion away from the interface into the alloy, there to precipitate internal sulphide particles.

In the presence of H_2O(g), even more sulphur is incorporated into the scale, again almost all at grain boundaries. Water vapour also leads to oxide grain refinement and accelerated inward oxygen transport, reflecting effects of H_2O-derived species on the oxide grain boundaries. The presence of these species on the boundaries is suggested to enhance sulphur uptake, but the mechanism is unknown.

A second effect of H_2O(g) is the suppression of internal sulphidation. Annealing experiments in the absence of sulphur showed that alloy

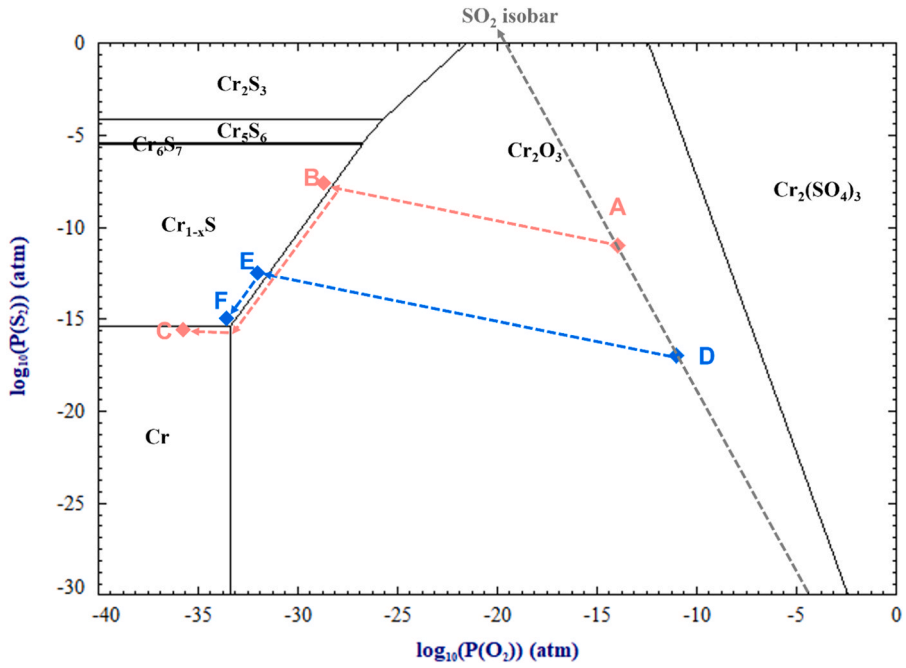

Fig. 14. Cr-S-O predominance diagram at 650 °C calculated using FactSage 8.1. Point A and D represent the gas phase conditions at the scale surface in dry and wet SO_2 gas, respectively. Dotted lines A-B-C and D-E-F represent assumed diffusion paths for oxygen and sulphur from gas/scale to scale/alloy in dry and wet SO_2 gas, respectively.

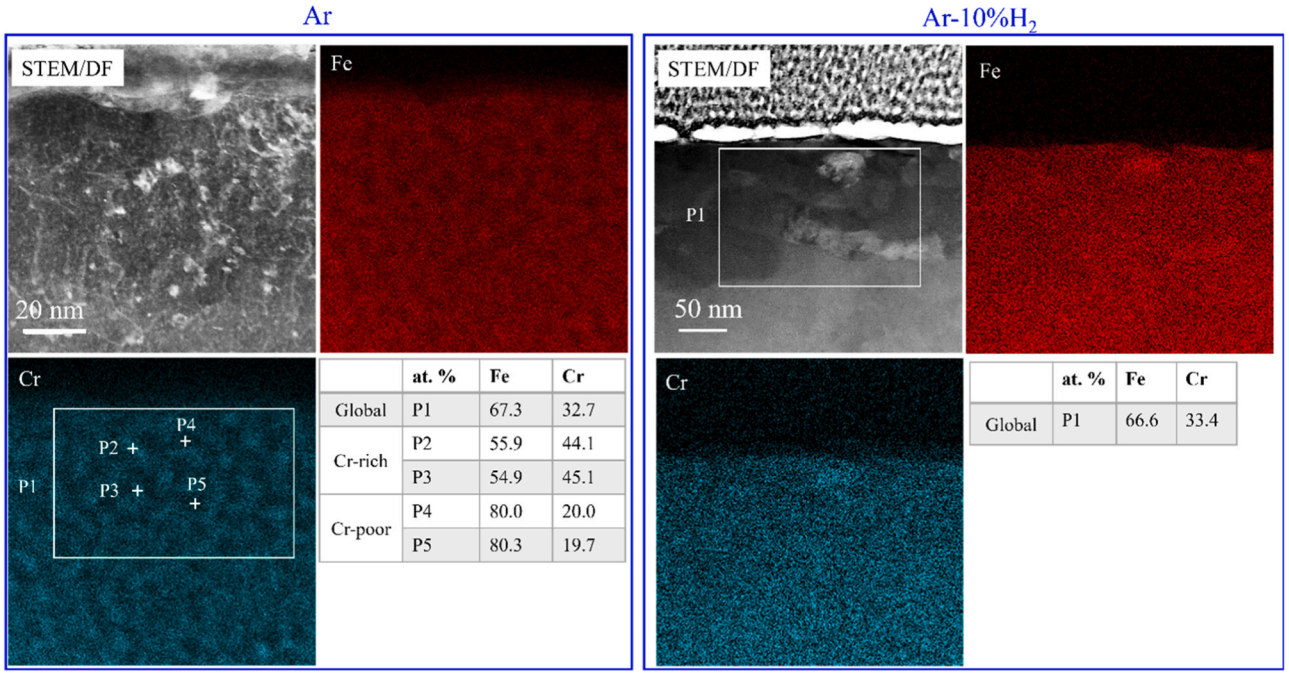

	at. %	Fe	Cr
Global	P1	67.3	32.7
Cr-rich	P2	55.9	44.1
	P3	54.9	45.1
Cr-poor	P4	80.0	20.0
	P5	80.3	19.7

	at. %	Fe	Cr
Global	P1	66.6	33.4

Fig. 15. STEM/EDS analysis of Fe-30Cr alloy annealed in Ar and Ar-10%H_2 650 °C for 100 h.

decomposition to precipitate the Cr-rich σ-phase occurred in H-free environments, but was much less obvious when hydrogen was present. The formation of a Cr-rich phase in one case but not the other provides a possible explanation for internal sulphidation only in the H-free SO_2 environment.

Sulphur uptake by the alloy can be avoided at least in short term by pre-oxidation in S-free H_2O(g) prior to exposure to SO_2. Although S-species are evidently unable to enter oxide grain boundaries produced in this way, grain boundary oxygen continues to be mobile, as evidenced by the subsequent growth of additional chromia beneath the pre-oxidation scale.

CRediT authorship contribution statement

Chuhan Sha: Conceptualization, Methodology, Investigation, Data Curation, Writing - Original Draft, **Limei Yang:** APT sample preparation, **Julie M. Cairney:** Writing - Review & Editing, **Jianqiang Zhang:** Supervision, Writing - Review & Editing, Funding acquisition, **David J. Young:** Writing - Review & Editing, Funding acquisition.

Declaration of Competing Interest

The authors declare that they have no known competing financial interests or personal relationships that could have appeared to influence the work reported in this paper.

Data availability

No data was used for the research described in the article.

Acknowledgement

Financial support by Australia Research Council under Discovery Project Scheme is gratefully acknowledged.

References

[1] G.R. Holcomb, et al., Fireside corrosion in oxy-fuel combustion of coal, ECS Trans. 41 (42) (2012) 73.
[2] Buckthorpe, D., J. Baker, and P. Sherlock. Materials for Advanced Gas-cooled Nuclear Systems. in Advanced Materials Research. 2009. Trans Tech Publ.
[3] S.C. Okoro, et al., Complementary methods for the characterization of corrosion products on a plant-exposed superheater tube, Metallogr. Microstruct. Anal. 6 (1) (2017) 22–35.
[4] L. Rosendahl, Biomass Combustion Science, Technology and Engineering, Elsevier,, 2013.
[5] C. Wagner, Theoretical analysis of the diffusion processes determining the oxidation rate of alloys, J. Electrochem. Soc. 99 (10) (1952) 369.
[6] G.H. Meier, et al., Effect of alloy composition and exposure conditions on the selective oxidation behavior of ferritic Fe–Cr and Fe–Cr–X alloys, Oxid. Met. 74 (5) (2010) 319–340.
[7] C. Fujii, R. Meussner, Carburization of Fe-Cr Alloys During Oxidation in Dry Carbon Dioxide. J. Electrochem. Soc. 114 (5) (1967) 435.
[8] H. Ma, C. Zhou, L. Wang, High temperature corrosion of pure Fe, Cr and Fe–Cr binary alloys in O2 containing trace KCl vapour at 750° C, Corros. Sci. 51 (8) (2009) 1861–1867.
[9] M.H.B. Ani, et al., The effect of water vapor on high temperature oxidation of Fe-Cr alloys at 1073 K, Mater. Trans. 50 (11) (2009) 2656–2663.
[10] G. Cao, et al., High temperature oxidation of Fe-Cr alloys in atmospheres containing 2.0% SO2+ 5.0% O2, Corros. Sci. 187 (2021), 109481.
[11] S. Mrowec, The problem of sulfur in high-temperature corrosion, Oxid. Met. 44 (1) (1995) 177–209.
[12] X. Zheng, D. Young, High temperature corrosion of pure chromium in CO-CO_2-SO2-N2 atmospheres, Corros. Sci. 36 (12) (1994) 1999–2015.
[13] C. Stephan-Scherb, et al., Comprehensive insights into competitive oxidation/sulfidation reactions on binary ferritic alloys at high temperatures, Corros. Sci. 203 (2022), 110236.
[14] M. Benlyamani, F. Ajersch, G. Kennedy, Solubility of sulfur in pure Cr2O3 at 1000° C, Oxid. Met. 29 (3) (1988) 203–216.
[15] T.D. Nguyen, et al., Atom probe study of impurity segregation at grain boundaries in chromia scales grown in CO_2 gas, Corros. Sci. 132 (2018) 125–135.
[16] D.J. Young, et al., Penetration of protective chromia scales by carbon, Scr. Mater. 77 (2014) 29–32.
[17] Perry, R.H., D.W. Green, and J. Maloney, *Perry's Chemical Engineers' Handbook (ed.)*. Seventh, International edition, 1997.
[18] H. Rau, The chromium-sulphur system between 873 K and 1364 K, J. Less Common Met. 55 (2) (1977) 205–211.
[19] R. Lobnig, H. Grabke, Mechanisms of simultaneous sulfidation and oxidation of Fe-Cr and Fe-Cr-Ni-alloys and of the failure of protective chromia scales, Corros. Sci. 30 (10) (1990) 1045–1071.
[20] X. Zheng, D. Young, Sulphide formation after pre-oxidation of chromia formers, Corros. Sci. 38 (11) (1996) 1877–1897.
[21] F. Falk, O. Sobol, C. Stephan-Scherb, The impact of the microstructure of Fe-16Cr-0.2C on high-temperature oxidation–sulphidation in SO2, Corros. Sci. 190 (2021), 109618.
[22] T. Narita, T. Ishikawa, Internal sulphidation phenomena of heat-resistant alloys at low sulphur pressures, Mater. Sci. Eng. A 120 (1989) 31–38.
[23] K. Nützmann, et al., Identification and 3D reconstruction of Cr5S6 precipitates along grain boundaries in Fe13Cr, Jom 70 (8) (2018) 1478–1483.
[24] R. Lobnig, et al., Diffusion of cations in chromia layers grown on iron-base alloys, Oxid. Met. 37 (1) (1992) 81–93.
[25] J.H. PARK, W.E. King, S.J. ROTHMAN, Cation tracer diffusion in Cr2O3 and Cr2O3–0.09 wt% Y2O3. J. Am. Ceram. Soc. 70 (12) (1987) 880–885.
[26] Graham, M.J., et al. Anion transport in growing Cr2O3 scales. in Materials science forum. 1989. Trans Tech Publ.
[27] D.J. Young, High Temperature Oxidation and Corrosion of Metals 1, Elsevier, 2016.
[28] Flatley, T. and N. Birks, JISI, 209, 523 (1971). F. Gesmundo, C. Asmundis, S. Merlo, & C. Bottino: Werkst. Korros, 1979. 30: p. 179.
[29] F. Gesmundo, D. Young, S. Roy, The high temperature corrosion of metals in sulfidizing-oxidizing environments: a critical review, High. Temp. Mater. Process. 8 (3) (1989) 149–190.
[30] Kofstad, P., High temperature corrosion. Elsevier Applied Science Publishers, Crown House, Linton Road, Barking, Essex IG 11 8 JU, UK, 1988., 1988.
[31] S.-H. Choi, J. Stringer, The breakaway corrosion of Fe-Cr alloys in atmospheres containing sulfur and oxygen, Mater. Sci. Eng. 87 (1987) 237–242.
[32] M. Hänsel, W. Quadakkers, D. Young, Role of water vapor in chromia-scale growth at low oxygen partial pressure, Oxid. Met. 59 (3) (2003) 285–301.
[33] G. Raynaud, R. Rapp, In situ observation of whiskers, pyramids and pits during the high-temperature oxidation of metals, Oxid. Met. 21 (1) (1984) 89–102.
[34] B. Chattopadhyay, G. Wood, The transient oxidation of Fe-Cr and Ni-Cr alloys, J. Electrochem. Soc. 117 (9) (1970) 1163.
[35] C. Yu, J. Zhang, D.J. Young, Corrosion behaviour of Fe–Cr–(Mn, Si) ferritic alloys in wet and dry CO_2–SO2 atmospheres at 650° C, Oxid. Met. 90 (1) (2018) 97–118.
[36] S. Saunders, M. Monteiro, F. Rizzo, The oxidation behaviour of metals and alloys at high temperatures in atmospheres containing water vapour: A review, Prog. Mater. Sci. 53 (5) (2008) 775–837.
[37] Michalik, M., M. Hänsel, and W.J. Quadakkers, Effect of water vapour on growth and adherence of chromia scales on pure chromium. 2007: Forschungszentrum, Zentralbibliothek.
[38] W.D. Kingery, H.K. Bowen, D.R. Uhlmann. Introduction to Ceramics 17, John wiley & sons,, 1976.
[39] Y. Ustinovshikov, M. Shirobokova, B. Pushkarev, A structural study of the Fe-Cr system alloys, Acta Mater. 44 (12) (1996) 5021–5032.
[40] L. Niewolak, et al., Sigma-phase formation in high chromium ferritic steels at 650C, J. Alloy. Compd. 638 (2015) 405–418.
[41] H. Grabke, D. Wiemer, H. Viefhaus, Segregation of sulfur during growth of oxide scales, Appl. Surf. Sci. 47 (3) (1991) 243–250.